Applied Surface Science 507 (2020) 145038

Contents lists available at ScienceDirect

Applied Surface Science

journal homepage: www.elsevier.com/locate/apsusc

Full Length Article

Graphene and graphene oxide as adsorbents for cadmium and lead heavy metals: A theoretical investigation

Sara M. Elgengehi[a], Sabry El-Taher[a], Mahmoud A.A. Ibrahim[b], Jacques K. Desmarais[c], Khaled E. El-Kelany[d,b,*]

[a] Department of Chemistry, Faculty of Science, Cairo University, 12613 Giza, Egypt
[b] CompChem Lab, Chemistry Department, Faculty of Science, Minia University, 61519 Minia, Egypt
[c] Dipartimento di Chimica, Università di Torino, Via P. Giuria 5, 10125 Torino, Italy
[d] Institute of Nanoscience and Nanotechnology, Kafrelshiekh University, 33516 Kafrelskiekh, Egypt

ARTICLE INFO

Keywords:
Graphene
Graphene oxide nanomaterials
Heavy metal adsorption
Water purification
Density functional theory
Dispersion

ABSTRACT

The geometrical and electronic parameters for the interaction of two toxic heavy metals, namely: cadmium (Cd) and lead (Pb), on graphene and graphene oxide (GO) surfaces are investigated by using local Gaussian type basis sets and the hybrid PBE0 functional as implemented in the CRYSTAL code. The role of including long-range dispersion (D3) contribution as well as the basis set superposition error (BSSE) on the adsorption process is found to be crucial in the description of such interactions. Generally, Cd and Pb adatoms are found to be adsorbed more strongly on GO rather than pristine graphene due to the incorporation of oxygen functional groups (epoxy and/or hydroxyl) on the surface. Moreover, Pb has interestingly been found to play as an electron donor and to form covalent bonding with the GO surface. Such findings could have an impact in water treatment applications using graphene-based nanomaterials.

1. Introduction

Since the discovery of graphene in 2004 [1], it has become an essential material in a wide range of research and technologies due to its special properties. One of its important features is that, it has a unique electronic band structure with zero band gap [2]. This leads to its excellent electrical transport and its fast charge mobility [3,4]. Moreover, graphene has a high thermal conductivity, a high strength, a large specific surface area (2630 m^2/g), it is biocompatible and it can be easily functionalized to improve its properties and extend its applications [5–7]. Because of these exceptional properties, graphene and modified graphene have been studied in various application fields such as sensors [8–10], catalysis [11–13], energy storage [14,15], electronics [16–18], biomedical [19,20] and water remediation [21–23].

Nowadays, heavy metal pollution is a growing public health concern. There are many efforts to get rid of these metals such as cadmium (Cd) and lead (Pb) due to their carcinogenicity and toxicity. Among the various methods used to remove heavy metals, adsorption has shown to be the most powerful process, because it is environmentally friendly and relatively efficient [24]. Owing to the large surface area of graphene, it can be a good adsorbent for different pollutants [25]. Unlike graphene, graphene oxide (GO) has different oxygen-containing functional groups which can act as binding sites for heavy metals. Also, GO is easily dispersed in water, it is hydrophilic, it has fast kinetics and a higher surface area than pristine graphene. Therefore, GO has high adsorption capacity for heavy metals removal [26,27] and in general is a good candidate for water treatment and desalination [28–30].

Utilizing graphene and graphene derivatives in heavy metals removal requires a good understanding of the nature of bonding. Therefore, several theoretical studies on the adsorption of metals on graphene have been carried out since its discovery. For example, Nakada and Ishii studied the adsorption for most elements using the local density approximation (LDA) of the density functional theory (DFT) [31]. They reported that the adsorption energy of elements with filled d- and s-orbitals, as in Cd, is very small and that adsorption is accompanied with a minimum migration energy. However, in their research spin polarization was not considered. Moreover, Manadé et al. [32] have considered the van der Waals (vdW) dispersive forces using Grimme's D2 dispersion correction along with the PBE functional for the interaction of 3d, 4d and 5d transition metals with the graphene surface for only one coverage of 0.031 monolayer (ML).

For Pb adsorption on graphene, the bond character and preferred site for metal adsorption have been previously investigated using spin-polarized DFT [33]. The Pb atom is found to prefer positioning on top of

* Corresponding author at: Institute of Nanoscience and Nanotechnology, Kafrelshiekh University, 33516 Kafrelskiekh, Egypt
E-mail addresses: kh.e.elkelany@gmail.com, khaled.elkelany@unito.it (K.E. El-Kelany).

https://doi.org/10.1016/j.apsusc.2019.145038
Received 16 September 2019; Received in revised form 28 November 2019; Accepted 10 December 2019
Available online 12 December 2019
0169-4332/

the graphene carbon atoms, with a mixed ionic and covalent character. At low temperature, Pb can easily migrate on the graphene surface, then forms small clusters [34]. Lately, the adsorption of Cd, Hg and Pb was investigated by Shtepliuk et al. [35] in a search for graphene-based heavy metals sensors. The B3LYP and PBE-D3 functionals have been applied by these authors to analyze the interaction of the aforementioned heavy metals with graphene quantum dots and extended graphene, respectively. It has been found that Pb binds more strongly than Cd and Hg and acts as an electron donor. Unlike Pb, Cd and Hg do not tend to form clusters on the surface of graphene.

To date, few theoretical studies have been done on the adsorption of Cd and Pb on graphene oxide (GO). It is obvious that the presence of carboxyl or hydroxyl functional groups on the graphene sheet increases the adsorption stability with respect to pristine graphene. For instance, previous DFT calculations were utilized for the study of the interaction of Pb and Zn atoms with carboxylated and hydroxylated graphene sheets, and the hydroxyl group was found to be more effective in the stabilization of the adsorption process of both metals [36].

In the current study, we use periodic DFT and Gaussian type function basis sets to study the adsorption of two heavy metals that cause water pollution, namely: Cd and Pb onto graphene monolayers. Here, different sizes of graphene supercells are considered to examine the effect of coverage on both adsorption energies and geometries. The effect of these metals on the electronic properties of graphene has been investigated by analyzing density of states (DOS) diagrams and Mulliken (confirmed by Hirshfeld) populations. In order to fill the gap of the past reports, as the adsorption of Cd and Pb on GO has not been fully elucidated, three models of GO with the most favourable coverages and configurations found by Boukhvalov et al. [37] have been considered to examine the enhancement in the adsorption process. The changes in the structure of GO, the DOS diagram, and the charge population have also been studied. Finally, the role of DFT-D3 correction of dispersion interactions on the adsorption process of both Cd and Pb on graphene and GO is considered. Herein, the solvent effect is not considered due to software limitation, while according to recent previous studies on graphene-like-structure (coronene and graphene quantum dots) [38], it is expected that the relative stabilities if not improved will be at least preserved.

2. Computational methods

Periodic restricted (closed shell) and unrestricted (spin-polarized) DFT calculations have been performed using the CRYSTAL17 [39,40] software to obtain the optimal geometries and electronic properties of Cd-graphene and Pb-graphene, respectively. All DFT calculations have been carried out using PBE0 [41], a hybrid and parameter-free functional. Indeed, PBE0 has proved to be effective in describing extended systems [42]. All-electron basis sets are used for all atoms except Cd and Pb, for which effective core potentials (ECP) are used [43,44]. Carbon and oxygen atoms in graphene and GO are described by the modified m-6-311G(d) basis set [43], while hydrogen atoms are described by the 6-31G(d,p) basis set [45].

The truncation of the Coulomb and exchange infinite lattice sums is controlled by five thresholds, which are here set to 7, 7, 7, 9, and 30 (see CRYSTAL manual in Ref. [40] for exact details). The numerical integration accuracy of the DFT exchange-correlation potential and energy is evaluated via a pruned grid (keyword XLGRID in Ref. [40]) which is represented by 75 radial and 974 angular points for each radial point. The self-consistent field (SCF) energy convergence threshold value in all of our calculations was set to 10^{-8} Hartrees. A 0.001 Hartree Fermi smearing parameter is applied for calculations on pure semiconducting graphene. A 12 × 12 × 1 Monkhorst-Pack/Gilat grid of k-points was used to represent the integration in the first Brillouin zone. Charge transfer between adatoms and graphene or GO was calculated using Mulliken and Hirshfeld population analysis [46,47]. Electron charge density difference maps were plotted using the graphical CRYSPLOT platform [48].

All geometry optimizations were carried out at first with PBE0, then the conformations of each adatom-substrate system were re-optimized using the PBE0-D3 functional in order to account for the long range vdW interactions with D3 Grimme correction [49]. For any heavy metal adsorbed on graphene or GO, the adsorption energy (E_{ads}) is defined as

$$E_{ads} = E_{G/GO\text{ - }HM} - E_{G/GO} - E_{HM}$$

where $E_{G/GO\text{-}HM}$ is the total energy of the complex, $E_{G/GO}$ is the total energy of pristine graphene or GO and E_{HM} is the total energy of the heavy metal alone in the same initial geometry of the adatom-substrate system. Here, the Boys and Bernardi counterpoise method is considered to account for basis set superposition errors (BSSE). The correction is achieved by using ghost atoms in the calculation of binding energies [50,51].

$$E_{ads}(\text{BSSE}) = E_{ads} + \text{BSSE}$$

and

$$\text{BSSE} = [E_{G/GO}(\text{system}) - E_{G/GO}(\text{ghost})] + [E_{HM}(\text{system}) - E_{HM}(\text{ghost})]$$

where $E_{G/GO}$ (ghost) and $E_{G/GO}$ (system) are the energies of only graphene/GO at the geometry adopted of the complex system with and without ghost atoms for adatom, and similarly for the E_{HM} (ghost) and E_{HM} energies of the heavy metal.

3. Results and discussion

3.1. Pristine graphene

3.1.1. Geometrical and energetical properties

Here, we consider different graphene supercells that are built as 2 × 2, 3 × 3, 4 × 4, 5 × 5, 6 × 6 and 7 × 7 expansions of the graphene primitive cell. The supercells contain 8, 18, 32, 50, 72 and 98 carbon atoms respectively, see Fig. 1(a). As one heavy metal is placed on each graphene supercell, the following adatom surface coverages (x) are accordingly realized: 0.125 (1/8), 0.056 (1/18), 0.031 (1/32), 0.020 (1/50), 0.014 (1/72) and 0.010 (1/98) ML. The adsorption of Cd and Pb has been studied on three different highly symmetric graphene sites, namely: hollow (H), bridge (B) and top (T) as shown in Fig. 1(b). Firstly, the PBE0 results are introduced in Table 1, where the geometrical properties of the different coverages (x) are reported. For each adatom, Table 1 encompasses the most stable site and the equilibrium adatom height (h), that is calculated as the difference between the z coordinate of the adatom and the average z coordinates of the carbon atoms in the graphene supercell, together with a quantification of the graphene sheet distortion. This distortion is calculated by subtracting the maximum and minimum displacement of the graphene carbon atoms through the z direction. The reported most stable site shows that Cd prefers to adsorb on the H site in all studied coverages, which is consistent with the results of Nakada et al. [52]. Furthermore, the energy barrier for Cd to diffuse from B or T site to H site is ~5 meV, which is negligible. Due to this small energy barrier, the three adsorption sites can be nearly considered as isoenergetic, and consequently the preferred adsorption site of Cd on graphene is strongly dependent on the applied computational method [32]. For Pb adsorption, the T site is the preferred one, in all but one case. It is noticed that as the coverage is decreased, Pb diffuses from T site to B site when x = 0.010 ML. The diffusion barrier between these two positions is very negligible, so that one of the two preferred sites (B or T site) is a transition state of the other during the relaxation of the geometry. This is consistent with what is previously concluded [53], that both the T and B sites are energetically favorable for large IVA group atoms like Pb when adsorbed on graphene.

Comparing the height of both adatoms from the graphene sheet, we find that Pb adsorbs at shorter distances than Cd and this is consistent with the calculated adsorption energies (Table 2). The PBE0

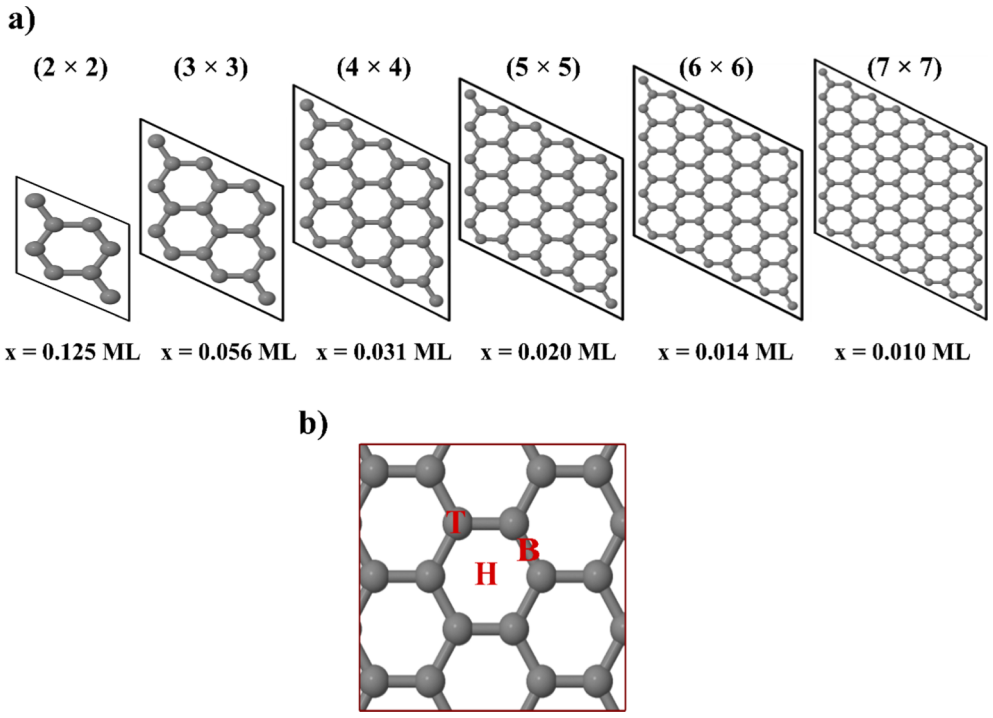

Fig. 1. Graphical representation of a) different supercells of graphene with their corresponding coverage (x) values when one adatom is placed and b) the studied adsorption sites on each graphene supercell, where H, B, and T stand for hollow, bridge, and top sites, respectively.

Table 1
Geometrical properties of the most stable site for different coverages of the adatom. The most stable adsorption site, adatom equilibrium height (*h*), and distortion of graphene layer are listed for each coverage (x). H, T, and B refer to hollow, top, and bridge adsorption sites, respectively. Calculations are performed using the PBE0 functional.

x (ML)	Most stable site		*h* (Å)		Distortion (Å)	
	Cd	Pb	Cd	Pb	Cd	Pb
0.125	H	T	3.737	2.592	0.011	0.044
0.056	H	T	3.637	2.600	0.011	0.092
0.031	H	T	3.631	2.633	0.013	0.145
0.020	H	T	3.604	2.630	0.026	0.161
0.014	H	T	3.587	2.637	0.030	0.109
0.010	H	B	3.629	2.647	0.009	0.180

calculations show that there are minimal differences for the adsorption heights between the different coverages of heavy metals, for example: *h* values vary in the range 3.59–3.74 Å (2.59–2.65 Å) for Cd (Pb), respectively. Distortion values rely on the site preference, as shown in Table 1. For instance, adsorption of Cd on the H site induces a small deviation from the graphene planarity with values around 0.01–0.03 Å. In contrast for adsorption of Pb on the T or B site, where binding to graphene is stronger, the attached carbon atom(s) shift upwards with much larger distortion values range from 0.04 to 0.18 Å. Generally, we noticed that the local distortion increases as the size of the graphene sheet increases. The larger the supercell size, the more concentrated will be the deformation around the adsorption area leaving the further carbon atoms less perturbed, in contrast to the smaller supercells, where the deformation is spreaded over almost all atoms.

For the analysis of energetical properties, we report information on adsorption energies (E_{ads}, eV) with and without BSSE, Mulliken charge transfer and band gaps (BG, eV) in Table 2. As shown, the adsorption

Table 2
Energetic and electronic properties of the most stable site for different coverages of the adatom. Uncorrected and corrected adsorption energies are calculated as previously reported in the Computational details section. ΔQ is the Mulliken charge transfer and the Hirshfeld charge transfer which are given between parentheses. Negative charge values mean that the metal acts as an acceptor and the opposite for positive values. BG is the band gap in eV. All calculations are done using the PBE0 functional.

x (ML)	E_{ads} (eV)		E_{ads} − BSSE (eV)		ΔQ		BG (eV)	
	Cd	Pb	Cd	Pb	Cd	Pb	Cd	Pb
0.125	−0.083	−0.739	0.015	0.109	−0.033 (−0.015)	0.197 (0.482)	0.075	–
0.056	−0.101	−0.764	0.016	0.094	−0.040 (−0.023)	0.260 (0.544)	0.055	–
0.031	−0.103	−0.790	0.015	0.081	−0.041 (−0.024)	0.341 (0.612)	0.019	–
0.020	−0.106	−0.851	0.015	0.036	−0.043 (−0.026)	0.419 (0.695)	0.013	–
0.014	−0.110	−0.797	0.013	0.088	−0.045 (−0.027)	0.367 (0.642)	0.015	–
0.010	−0.097	−0.956	0.021	−0.061	−0.042 (−0.025)	0.525 (0.794)	–	–

energy of Cd is very weak (~ −0.1 eV) without BSSE correction. This can be due to the stability of the electronic configuration of Cd, which has fully occupied d and s orbitals, and hence its binding stability with graphene is small. This finding is in agreement with that of Zólyomi et al. [54], who found that the binding energy decreases as the occupation of 4d and 5d shells in transition metals increases. On the other hand, the Pb adsorption energy is lower than that of Cd by about 0.7 eV without BSSE-correction. Indeed, Pb has 2 unpaired electrons in its outermost 6p orbital which can be the reason for its larger binding strength. This trend in E_{ads} is verified, as discussed above, by the larger adsorption height of Cd, compared to Pb. Moreover, the calculated Mulliken charges emphasize a charge transfer of about 0.20–0.53|*e*| from the Pb to the graphene sheet. However, an opposite behavior is found for Cd, where a very small charge (nominal value of 0.03–0.05|*e*|) are transferred to Cd. This reflects the very weak adsorption strength of Cd. In order to confirm charge-transfer direction, Hirshfeld charges are additionally calculated and reported in Table 2. While the numerical values of atomic charges obtained by Hirshfeld scheme are completely different from Mulliken ones, the main behaviour is confirmed and the charge transfer direction is maintained.

Since the adsorption of these heavy metals probably involves vdW forces, the inclusion of D3 dispersion correction is substantial to describe their adsorption on graphene more accurately [55]. An enhancement is noticed in both the geometries and energies of adatom-graphene systems by using the PBE0-D3 functional, see Table 3. The addition of D3 vdW correction has no effect on the preferred adsorbed site for both Cd and Pb. Nevertheless, the D3 correction has an important effect on the structural properties. These effects are more accentuated for Cd than Pb, the reduction in *h* values for Cd is about 0.5 Å. In contrast, the D3 correction increases the Pb equilibrium *h* values by 0.044 – 0.105 Å for the different coverages, except for the 0.010 ML coverage, in which *h* decreases by 0.059 Å. This decrease can be attributed to the change in the preferred adsorption site with respect to the previous coverage. As distortion is concerned, the addition of the dispersion correction minimizes graphene distortion in Pb-graphene systems by ~0.06 Å. However, for the Cd-graphene systems, the distortion increases by ~0.03 Å because the Cd atom gets closer to graphene when the D3 correction is applied. As discussed before, the distortion increases from 0.014 (0.038) Å to 0.093 (0.096) Å with decreasing the coverage from 0.125 ML to 0.010 ML for Cd (Pb)-graphene systems, respectively.

Moreover, Table 3 shows that the vdW correction shifts the E_{ads} to more negative values for Cd (Pb) by about 0.4 (0.6) eV in average, *e.g.* BSSE-uncorrected adsorption energies for Cd (Pb) on graphene with 0.031 ML coverage are −0.531 (−1.368) eV, respectively, compared to the D3-uncorrected/BSSE-uncorrected E_{ads} values of −0.103 (−0.790) eV. Both Mulliken and Hirshfeld charges also increase for Cd but not for Pb, see Table 3, with the same transfer direction as stated before. To account for BSSE, we employ the Boys and Bernardi counterpoise correction [50]. Calculated E_{ads} values are less negative after using the BSSE correction. In Table 2, it is noticed that after using this correction, adsorption energies become positive and even worse, Cd forms more stable complex with graphene than Pb. This behavior can be due to an overcorrection, as reported previously by Dimakis et al. [56] However, this is not the case when the PBE0-D3 functional is used, see Table 3, the trend in E_{ads} is maintained and the adsorption process is still favored.

Fig. 2 shows a relation between the BSSE-uncorrected E_{ads} and *h* values with coverage (x) for the Cd-graphene and the Pb-graphene systems calculated at the PBE0 and PBE0-D3 functionals. In general, we observed that the increased adatom coverages weaken the adatom-graphene interaction. Possible adatom-adatom vdW interactions are deduced from the decrease in adsorption strength as the coverage increases. These adatom-adatom interactions become very negligible at larger supercell sizes. A similar effect has been observed during a previous study of Li, Na, and K adsorption on graphene [57]. Fig. 2 shows that for Cd adsorbed on graphene, *h* gets larger as the coverage increases and this is consistent with the increase in the E_{ads} values. In contrast, the trend of *h* values for Pb-graphene with coverage at the PBE0 functional is opposite to that of the E_{ads} trend. This can be due to the poor description of the PBE0 functional for the Pb-graphene systems. However, this unexpected behavior of Pb disappears when the D3 correction (using instead the PBE0-D3 functional) is included. Additionally, the effect of increasing coverage, as revealed in Table 2 and Table 3, on charge transfer is consistent with the decrease in the adatom interaction with graphene. These findings emphasize the importance of using the D3 correction along with the PBE0 functional for such studies.

On closer inspection of the PBE0-D3 E_{ads} vs coverage graph, a sharp increase in the energy from x = 0.056 ML to x = 0.125 ML can be observed, in particular for the Cd adatom. This instability behaviour can be attributed to the higher lateral repulsion between the neighbouring adatoms (the distance to the next adatom is decreased from about 7.4 Å for x = 0.056 ML to about 4.9 Å in x = 0.125 ML). Otherwise, there is an abrupt energy decrease of 0.16 eV near x = 0.01 ML for Pb, which can be assigned to the shift in the preferred adsorption site between T and B site near this coverage value. Furthermore, a distinct behaviour (appearing as a local minimum or maximum for Cd and Pb, respectively) is noticed for x = 0.014 ML (supercell 6 × 6). This is a well-known peculiar behaviour [58–61], that exists in $n \times n$ supercells when *n* is a multiple of 3, and it is related to the four-folded degeneracy at the Γ point, instead of the double folded degeneracy at the K Dirac points for supercells that are not multiples of 3. This change in graphene symmetry causes exceptional trends in the adsorption

Table 3
Geometrical, energetic and electronic properties as a function of increasing supercell size for Cd/Pb adsorbed on graphene. Here, Grimme dispersion correction is considered, and calculations are obtained using the PBE0-D3 functional. Charge transfer ΔQ is calculated by using Mulliken and Hirshfeld (within parentheses) charges.

x (ML)	*h* (Å)		Distortion (Å)		E_{ads} (eV)		E_{ads} - BSSE (eV)		ΔQ		BG (eV)	
	Cd	Pb	Cd	Pb	Cd	Pb	Cd	Pb	Cd	Pb	Cd	Pb
0.125	3.212	2.697	0.014	0.038	−0.490	−1.278	−0.353	−0.488	−0.062 (−0.038)	0.183 (0.427)	0.074	–
0.056	3.135	2.676	0.024	0.062	−0.524	−1.346	−0.354	−0.529	−0.073 (−0.055)	0.241 (0.491)	0.065	–
0.031	3.114	2.687	0.038	0.084	−0.531	−1.368	−0.359	−0.534	−0.077 (−0.059)	0.313 (0.559)	0.019	–
0.020	3.099	2.675	0.049	0.084	−0.540	−1.421	−0.368	−0.575	−0.079 (−0.061)	0.387 (0.630)	0.013	–
0.014	3.093	2.681	0.054	0.051	−0.544	−1.383	−0.372	−0.540	−0.080 (−0.062)	0.349 (0.590)	0.018	–
0.010	3.069	2.588	0.093	0.096	−0.540	−1.541	−0.367	−0.638	−0.080 (−0.064)	0.534 (0.804)	0.0003	–

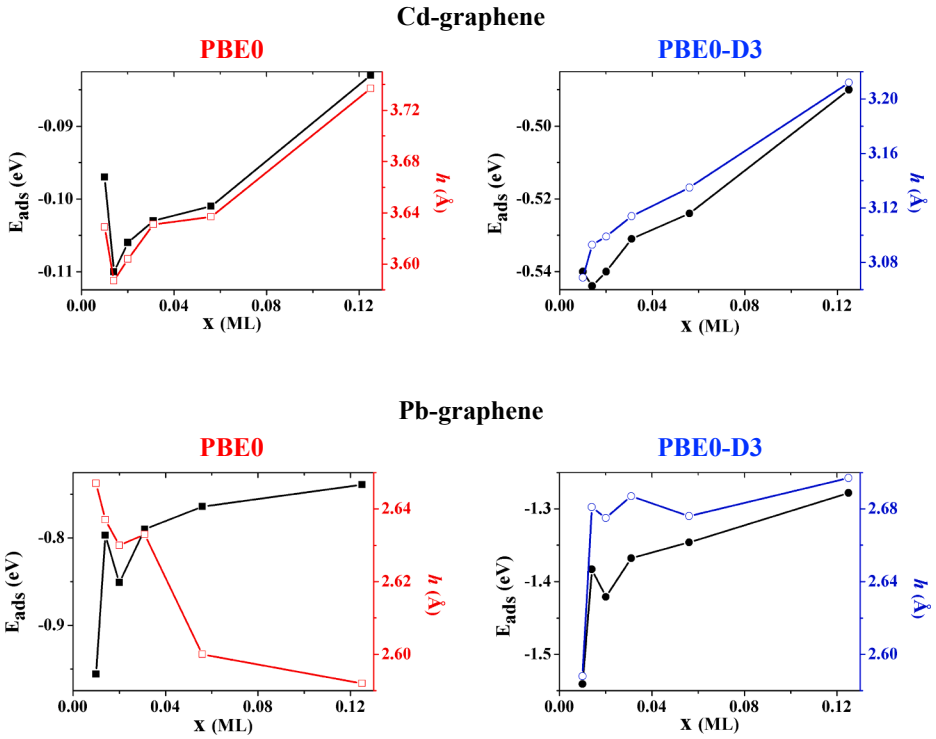

Fig. 2. Plots of adsorption energy E_{ads} (in eV) and adatom height *h* (in Å) for both Cd (up) and Pb (down) adsorbed on graphene versus adatom coverage with (right) and without (left) the D3 correction. Filled and empty squares (circles) represent E_{ads} and *h* values calculated by the PBE0 (PBE0-D3) functional, respectively.

energy for multiple of 3 supercells after introducing a perturbation like the adsorption of Cd or Pb.

3.1.2. Electronic properties analysis

In this section, the electronic structure of adatom-graphene systems is unfolded. Initially, the effect of the D3 correction on the DOS is shown in Fig. 3, which displays the total and projected DOS of the monomers in the optimized Cd/Pb-graphene (x = 0.031 ML) with and without the D3 correction. As demonstrated in Fig. 3, the D3 correction causes the states of Cd to be more populated and concentrated closer to the Fermi level, which results in a lower E_{ads} than that calculated using only PBE0. This observation verifies that the D3 correction is essential in the study of the adsorption behavior of Cd on graphene, and also its adsorption is mainly due to the dispersion interaction. The Pb adsorption behavior is similar to that of Cd in this respect. The dispersion correction affects the Pb states near the Fermi level to be slightly more populated and that causes more stabilization in the adsorption process.

In order to illustrate the effect of varying coverage on the DOS, the total and projected DOS spectra (Fig. 4) are computed for Cd/Pb-graphene optimized with the PBE0-D3 functional at the coverages of 0.125 ML, 0.02 ML, and 0.01 ML. We first analyze the DOS of the Cd-graphene system. It is noticed in the Cd-graphene DOS diagram that the Dirac point of graphene (where DOS is zero) coincides with the Fermi level and that adsorption of the Cd atom does not significantly change the DOS spectra of graphene. Some peaks appear below the Fermi level that correspond to 5s states of Cd. This behavior may reflect a sort of weak hybridization between the graphene sp states and the Cd s states. These Cd 5s peaks are more occupied in the adsorbed phase than in the isolated phase, which suggests that there is some charge transfer from graphene to Cd, in agreement with the above-mentioned discussion of Mulliken and Hirshfeld analysis. In fact, Dimakis et al. [56] found similar results for Zn which lies above Cd in the periodic table. These findings verify the lower adsorption strength of Cd on graphene. The effect of decreasing coverage on DOS is also investigated. It is found that the Cd DOS is broadened in the area below the Fermi level as coverage decreases. More specifically, the Cd peaks are more concentrated and less splitted near the Fermi level in Cd-graphene (x = 0.125 ML) but for lower coverages, the peaks are broadened until they become more condensed far below the Fermi level at a coverage of x = 0.01 ML.

Unlike Cd, Pb significantly alters the electronic structure of graphene and the Dirac point is no longer evident in the DOS diagram as shown in Fig. 4. From the diagram, it is obvious that there is a strong hybridization between sp states of both Pb and graphene around the Fermi level. This may be due to the formation of some degree of covalent bonding, which is in agreement with the results of Liu et al. [33]. Sometimes the location of the Dirac point relative to the Fermi level can help in the determination of the magnitude and direction of the charge transfer between the adatom and graphene [55]. However, in our case, since the Dirac point is no longer visible or coincides with the Fermi level in the Pb-graphene and Cd-graphene DOS, respectively, charge transfer cannot be determined using the former method. The DOS near the Fermi level in Pb-graphene are different for the up- and down-spin projections (Figs. 3 and 4), indicating the existence of a non-zero magnetic moment. For example, the adsorption of Pb on graphene with a coverage of 0.031 ML reduces the magnetic moment to 1.77 μ_B from 2.0 μ_B of the isolated atom. This value is in very good agreement with the previous studies of Pb adsorbed on graphene [33,34,53]. This reduction in magnetic moment is due to charge transfer from Pb to graphene which is equal to 0.313 in the case of the 0.031 ML coverage (Table 3).

In contrast to s peaks of Cd, sp peaks of Pb are above and below the Fermi level. As coverage decreases, the Pb peak near the Fermi level starts to become sharper, more expanded below the Fermi energy, and then it splits starting from the 0.031 ML coverage. As compared to the higher coverages, DOS of Pb-graphene at 0.01 ML coverage, has more than two peaks at range of − 0.87 to −1.5 eV away from the Fermi level and also a more diffuse peak appears around the Fermi energy. These additional peaks can cause more hybridization with graphene and stronger interaction which is indicated by the lower E_{ads}. Finally, Cd adsorption on graphene causes a very small gap opening (*e.g.* the gap ranges from 3.0×10^{-4} eV in x = 0.01 ML to 0.074 eV in x = 0.125 ML) whereas the corresponding systems due to Pb adsorption are still zero-gap semiconductors at all coverages.

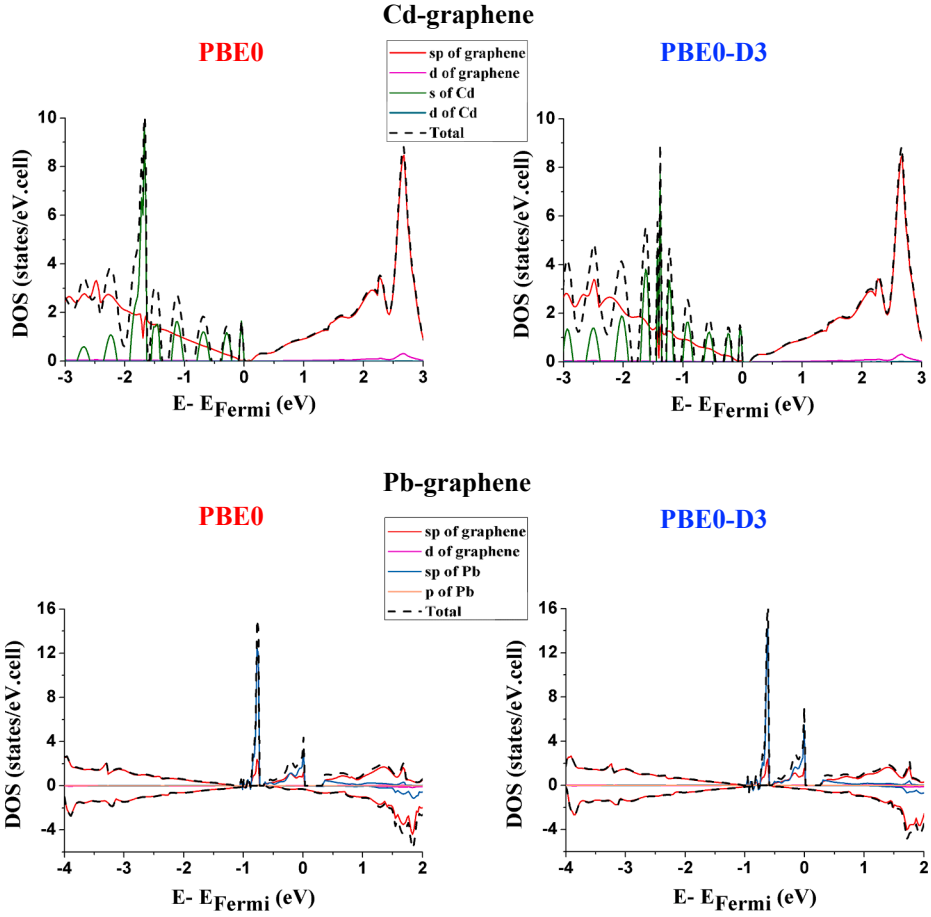

Fig. 3. Total and projected DOS diagrams for Cd-graphene (up) and Pb-graphene (down) systems calculated with the PBE0 (right) and PBE0-D3 (left) functionals. The projections onto various atomic orbitals are represented as different colored solid lines, whereas the total density of states is represented using a dashed line. The diagrams here are related to the adatom coverage of x = 0.031 ML (4 × 4 graphene supercell).

Fig. 5 shows the electron charge density difference maps (CDD) of (a) Cd-graphene and (b) Pb-graphene with PBE0-D3 at a coverage of 0.031 ML. This map is calculated as a difference with respect to a superposition of atomic densities. These plots verify that Pb interacts more strongly compared to Cd, *e.g.* there is some atomic density overlap between Pb and carbon atoms in the scale of the plot, which is absent in the Cd-graphene system. The CDD map for Cd-graphene system shows small electron density loss in the side of graphene with respect to Cd. However, the opposite is found for Pb-graphene, there is an increase in the electron density beside the carbon atom. Additionally, a spin density map in Fig. 5(c) shows that there is a decrease in the spin density on the carbon attached to the Pb atom, which is attributed to the charge transfer from Pb. The trends revealed in these plots are in good agreement with those of E_{ads}, charge population analysis and DOS diagrams.

3.2. Graphene oxide (GO)

3.2.1. Geometrical and energetical properties

The GO models proposed by Boukhvalov et al. [37], are considered here using a supercell expansion of 4 × 4 (x = 0.031 ML). Every model has different functional groups with the most stable coverages: 1) 100% epoxy (***E***) 2) 75% hydroxyl (***H***) and 3) 75% of both epoxy and hydroxyl groups (***B***), see Fig. 6. Many experimental studies have verified the existence of epoxy, hydroxyl groups and C—C double bonds in the GO structure [62–65]. However, in the studied GO models, edge groups are not taken into consideration because they are of minor amount. The mentioned oxygen functional groups lie above and below the surface of graphene and cause the graphene to lose its planarity. Moreover, OH groups in the (***H***) and (***B***) models tend to interact with each other forming hydrogen bonds that cause more distortion. Therefore, carbon atoms are puckered out of plane which leads to the appearance of some sp^3 hybridized carbon atoms. This coexistence of sp^2 and sp^3 carbon hybridization regions are confirmed experimentally by XPS spectroscopy [66]. According to that, our calculated bond lengths between functionalized carbon atoms are the highest for the (***H***) model which contains more OH groups, *i.e.* the bond length values for the (***E***), (***H***) and (***B***) models are 1.47 Å, 1.55 Å, and 1.53 Å, respectively, compared to 1.42 Å for pristine graphene (pure sp^2 hybridization).

Generally, for each GO model, the adatom can be positioned onto H site, B site, or T site, as previously introduced in Section 3.1 for pristine graphene. All possible adsorption sites for the 3 GO models are here considered. For clarity and to unambiguously label each site, numbers are used to represent the various adsorption positions on each GO model surface. Hence, **H** will refer to the positions on the hydroxyl model, **E** for epoxy, **B** and **b** for the upper and lower surfaces of epoxy-hydroxyl functionalized GO, respectively, as shown in Fig. 6. For instance, **E1** and **E2** introduce the hollow site of the adatom, while **E3, E4, E5** the bridge, and **E6**, **E7** the top, all of them with respect to graphene carbon atoms. The bridge epoxy **E3** configuration is found to be the most stable site for both the Pb and Cd adatoms. However, for hydroxyl and epoxy-hydroxyl GO models, the two adatoms Cd/Pb preferred different adsorption sites; **H9/H3** and **B4/b11**, respectively, see Fig. 6. Complete optimizations were performed at the PBE0-D3 level, where the numerical data for the most stable site of each GO model are given in Table 4. Geometrical parameters, as well as adsorption energies (E_{ads}) and differences with respect to the corresponding pristine graphene (ΔE) are given. The improvement in the adsorption energy is more pronounced for Pb than for Cd adatom with respect to pristine graphene. The Pb-GO (***B***) model is the most stable system with a difference of 2.141 eV (ΔE, BSSE-uncorrected) compared to pristine graphene. Pb in the previous configuration tends to form a

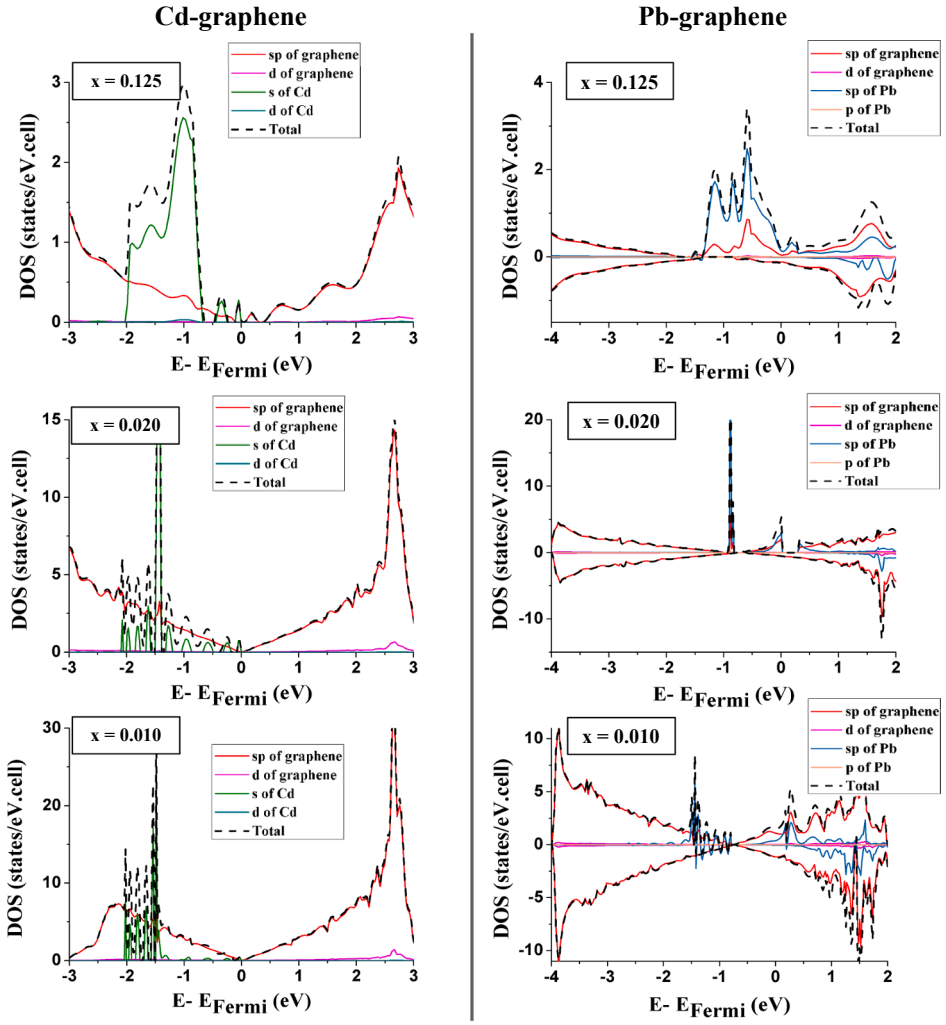

Fig. 4. Total and projected DOS diagrams for Cd-graphene and Pb-graphene systems using the PBE0-D3 functional at different coverages (values of x = 0.125, 0.020, and 0.010 ML) from top to bottom, respectively.

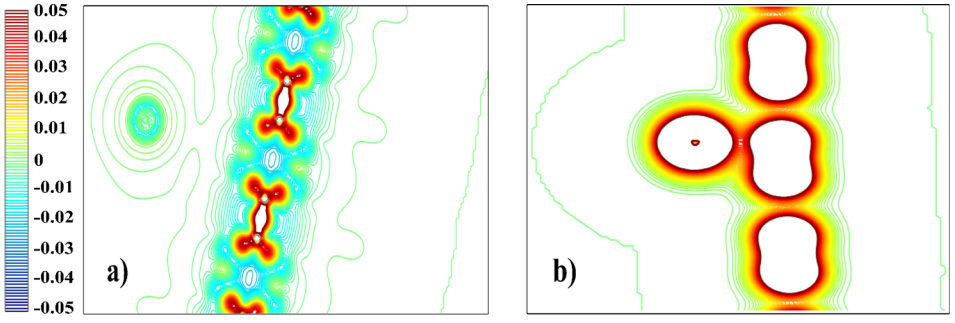

Fig. 5. Charge density difference (CDD) maps for a) Cd b) Pb adsorbed on graphene with x = 0.031 ML. The CDD maps are taken relative to the corresponding superposition of atomic densities in the *yz* plane. In CDD, the positive areas denote charge accumulation, while the negative areas denote charge depletion. A spin density map for the case of spin polarized Pb-graphene is additionally introduced in panel c.

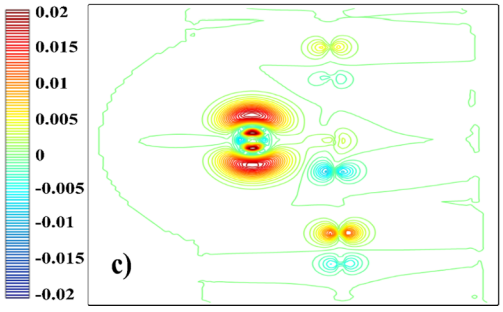

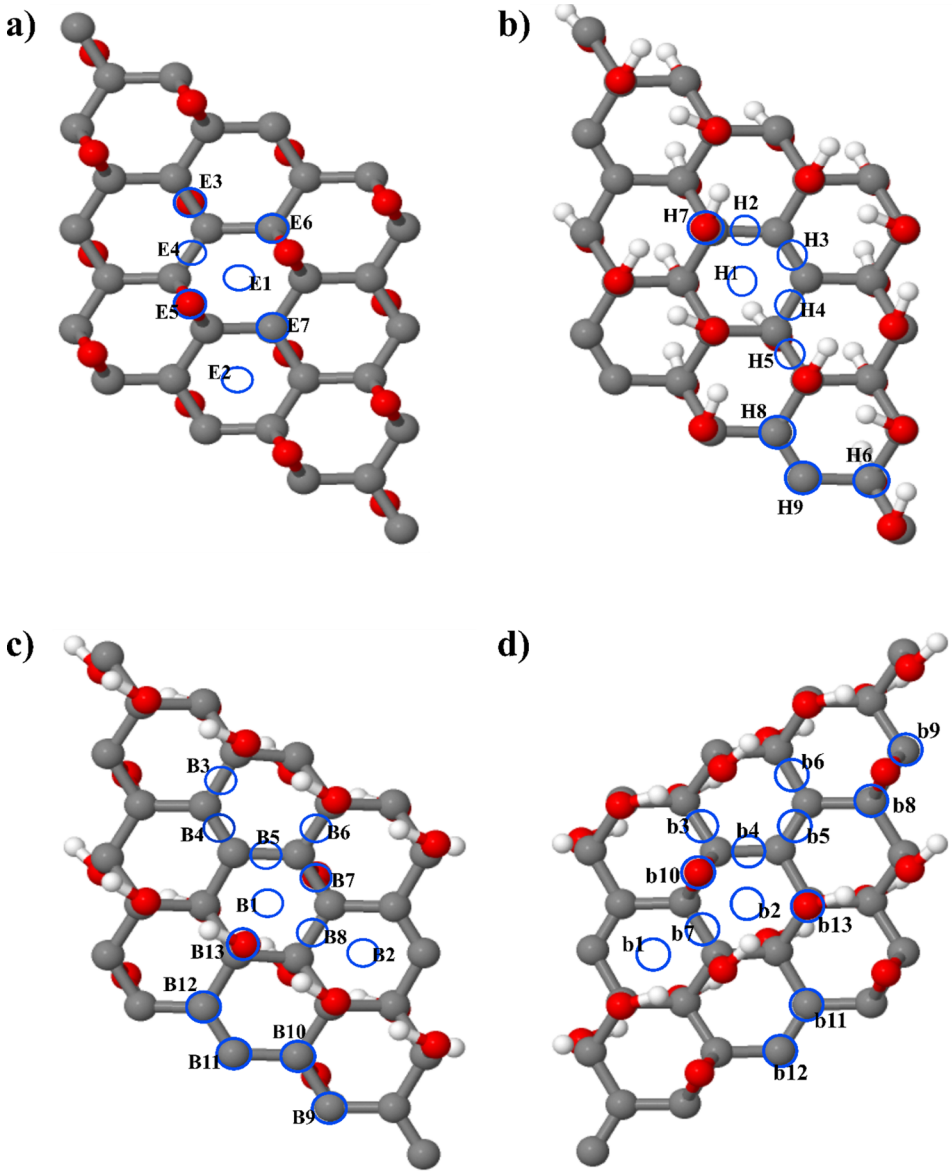

Fig. 6. Graphical representation of the considered adsorption sites on each GO model. E_{1-7} and H_{1-9} denote all possible sites for the *E*- and *H*- models; panels a and b. Possible sites for *B*-model are represented in panel c and d as B_{1-13} and b_{1-13} for its upper and lower surface, respectively.

bond with a close epoxy oxygen and this bond is equal to 2.16 Å. This epoxy oxygen gets distorted from its symmetrical bridge arrangement and detaches away from one carbon atom in order to form a new bond with Pb. The least stable system is Pb-GO (***E***) model, in which the difference between Pb-GO and Pb-graphene is almost negligible.

In the case of Cd adsorption on GO, the trend in the adsorption stability is a little different from that of Pb: Cd-GO (***H***) > Cd-GO (***B***) > Cd-GO (***E***). It is worth mentioning that binding energy values for

Table 4
Geometrical, energetic and electronic properties of the most stable structures of Cd/Pb-GO optimized with the PBE0-D3 functional. The adatom height (*h*) is calculated as the difference between the *z* coordinate of the adatom and the average *z* coordinates of the neighboring oxygen atoms. ΔE is the difference between the adsorption energy of the adatom on GO and graphene (x = 0.031 ML); $\Delta E = \{E_{ads}\ (GO) - E_{ads}\ (Graphene)\}$. ΔQ is the charge transfer calculated by Mulliken and Hirshfeld (within parentheses) schemes. BG is the band gap. Corrected-BSSE E_{ads} and ΔE are given in square brackets.

GO model	Most stable site		*h* (Å)		E_{ads} (eV)		ΔE (eV)		ΔQ		BG (eV)	
	Cd	Pb	Cd	Pb	Cd	Pb	Cd	Pb	Cd	Pb	Cd	Pb
(*E*) model	E3	E3	1.990	1.829	−0.563 [−0.349]	−1.375 [−0.425]	−0.032 [0.010]	−0.007 [0.109]	−0.006 (0.019)	0.179 (0.433)	4.343	1.974 (α) 6.051 (β)
(*H*) model	H9	H3	2.031	1.683	−0.689 [−0.403]	−1.942 [−0.702]	−0.158 [−0.044]	−0.574 [−0.168]	−0.025 (−0.008)	0.398 (0.741)	3.645	1.875 (α) 4.529 (β)
(*B*) model	B4	b11	1.988	1.078	−0.637 [−0.315]	−3.509 [−1.929]	−0.106 [0.044]	−2.141 [−1.395]	−0.092 (−0.032)	0.974 (0.904)	4.216	2.749 (α) 3.932 (β)

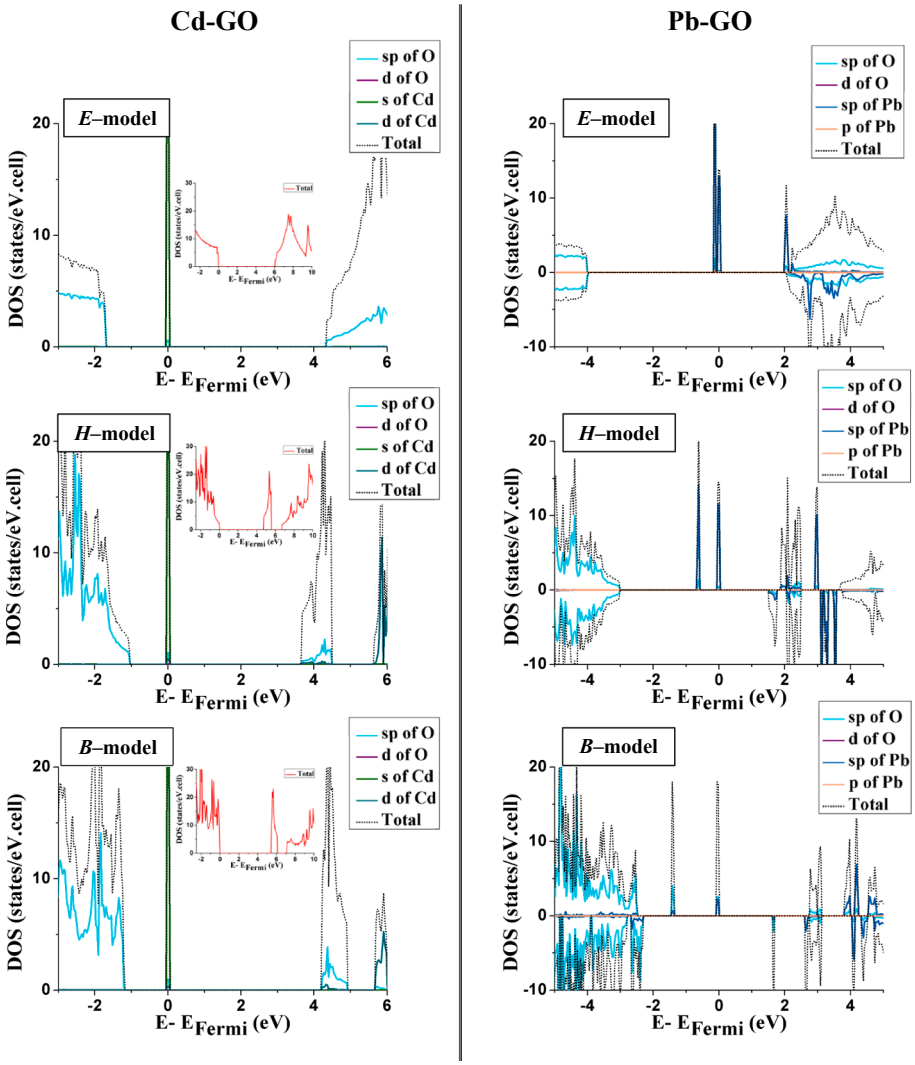

Fig. 7. Total and projected DOS diagrams for the different models of Cd-GO (left) and Pb-GO (right) systems. In order to elucidate the role of adsorption process on the DOS, total DOS of the corresponding pure GO is introduced as an inset (red lines) in each Cd-GO diagram.

the most stable Pb-GO and Cd-GO models are about 2.6 and 1.3 times that of the corresponding Pb-graphene and Cd-graphene systems, respectively. This implies that GO has a greater tendency to adsorb these heavy metals than pristine graphene. Therefore, the nature of Pb interaction with GO is chemisorption (E_{ads} = −3.509 eV) while for Cd, it is strong physisorption (E_{ads} = −0.689 eV). We noticed that the trend in BSSE-corrected E_{ads} is changed, for example: in the case of Cd, some adsorption energy differences became positive which indicates that some adatom-GO systems are less stable than graphene. This behavior can be attributed to the basis set overcorrection. A preliminary calculation of the adsorption energy for Pb-GO (***B***) and Cd-GO (***H***) without the D3 corrections gave the values of −1.2 eV and −0.168 eV, respectively. Therefore, the D3 correction incorporation causes E_{ads} results of Pb and Cd to be respectively almost 3 and 4 times the values without the dispersion. Epoxy groups in Pb-GO (***B***) geometry calculated with the PBE0 functional are symmetrical, whereas they are non-symmetric when the D3 correction is applied, because of the formation of Pb–O bond, which leads to the lowering in the E_{ads} (by an amount of ~2.3 eV). This result emphasizes again the vital role of dispersion interactions in the adsorption of these heavy metals.

The distance between adatom and the neighboring oxygen atoms plane *h* is calculated, as shown in Table 4. These distances for Pb are in general lower than those of Cd and in compliance with the values of E_{ads}. The values are on the order of 1.078 Å, 1.683 Å, and 1.829 Å for Pb-GO (***B***), Pb-GO (***H***), and Pb-GO (***E***), respectively. For the Cd case, the values of *h* have very small differences and are almost the same (~2.0 Å). A total charge of 0.974 |*e*| was transferred from Pb to GO in the most stable (***B***) model, but 0.025|*e*| was transferred from GO (***H***) model to Cd. This amount of charge transfer between Pb and GO is much higher than in pristine graphene, however, it is lower in the case of Cd, except for the (***B***) model of GO. Since GO is an insulating material [67], we noticed that the adsorption of these heavy metals reduces its band gap. For example, in the GO (***B***) model, Pb adsorption reduces its band gap to 2.749 eV and Cd adsorption on GO (***H***) configuration decreases the band gap to 3.645 eV. The calculated band gaps of pristine GO are 6.065 eV, 4.746 eV, and 5.447 eV for the GO (***E***), (***H***), and (***B***) models, respectively. Previous studies support our GO calculated band gaps [68,69].

3.2.2. Electronic properties analysis

Fig. 7 displays the total and projected DOS of Cd and Pb adsorbed on the different configurations of GO. At the Fermi level, Cd 5s states are the most dominant, with a very small O sp peak that could indicate a small hybridization between Cd s states and O sp states. The lower hybridization can explain the physisorption nature of Cd on GO. On the other hand, Pb-GO DOS shows strong hybridization between sp states of Pb and O sp states particularly in the (***B***) GO system where the DOS of GO is significantly altered. Beside the sp peaks of Pb around the Fermi

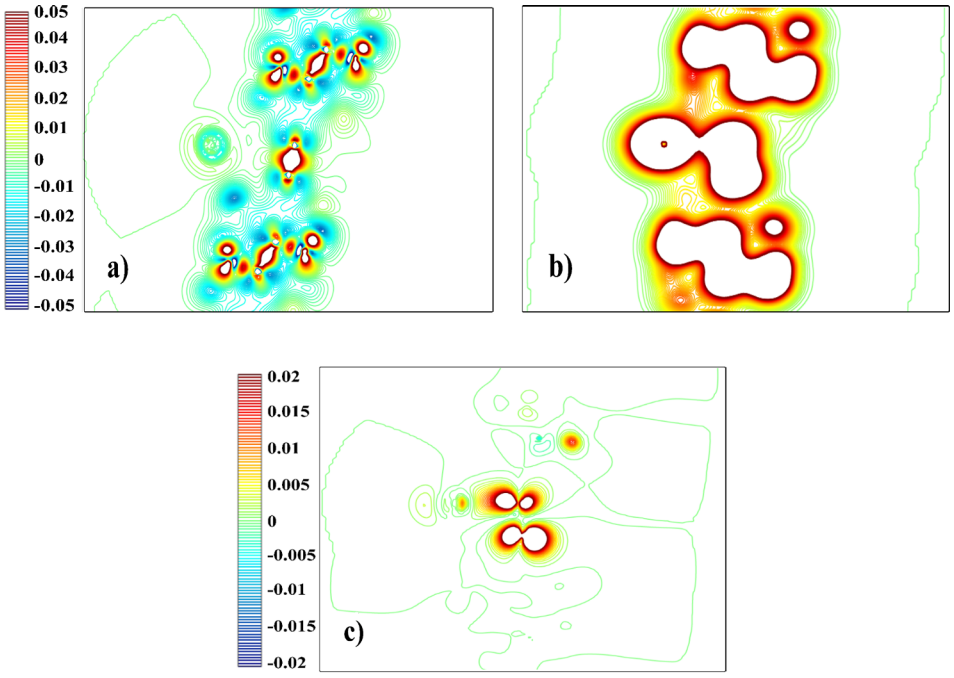

Fig. 8. CDD maps of the most stable model for Cd-GO (a) and Pb-GO (b). CDD plots are calculated relative to the corresponding superposition of atomic densities in the *yz* plane. In CDD, the positive areas denote charge accumulation, while the negative areas denote charge depletion. A spin density map of the spin polarized Pb-GO is also shown in panel c.

level, sp peaks of O appear which is indicative of the interaction between Pb and GO. Furthermore, electron charge density difference maps (CDD) of the most stable configurations of a) Cd-GO (***H***) and b) Pb-GO (***B***) are displayed in Fig. 8. From the low density depletion area around O atoms in GO (Fig. 8a), one can deduce that Cd accepts small amount of charge from the GO surface. However, in the Pb-GO (***B***) model map (Fig. 8b), the electron density is enriched around GO surface and there is visible charge transfer between the Pb and both O and C atoms. The spin density map (Fig. 8c) shows how the spin is lost from the Pb atom and is transferred to the GO (***B***) configuration and this is consistent with the largest amount of charge transfer from Pb to GO calculated previously. The magnetic moment is maintained to be 2.0 for all optimized Pb-GO systems.

4. Conclusions

In this paper, we have investigated the adsorption of two toxic heavy metals (Cd and Pb) on graphene and graphene oxide using periodic density functional theory (PBE0 functional). In order to study the effect of coverages, different sizes of graphene monolayers are considered. In general, Pb is found to adsorb more strongly on graphene than Cd and this result is supported by the calculated adatom height (*h*), Mulliken and Hirshfeld population analysis, DOS spectra and CDD maps. Moreover, because the migration energy of these metals is very low, it is believed that the adatom adsorption site preference depends on the nature of metal (adsorbate), the nature and size of the adsorbent and the calculation method, *e.g.* Cd prefers the H site, while Pb adsorbs on the T site (B site when x = 0.01 ML). It is observed that the increased adatom coverage is dominated by adatom-adatom lateral repulsions which weaken the adatom-graphene binding strength. This can be further explained by the presence of more peaks of the metal in the DOS spectra at lower coverages which increases the hybridization and the adatom-graphene interaction. A significant enhancement in the adsorption strength of these heavy metals after using D3 vdW correction stresses that dispersion is the dominant type of interaction. This enhancement in stability is further confirmed by the DOS diagram, where the states are more populated near the Fermi level. Additionally, a remarkable behavior is noticed in the adsorption of Cd or Pb on supercell expansions as multiples of 3 that can be attributed to a change of symmetry.

To overcome the relatively low adsorption energies especially for Cd, functionalization of graphene is adopted using different coverages of epoxy or/and hydroxyl groups. Our calculations proved that graphene functionalized with 75% of hydroxyl groups (75% of both epoxy and hydroxyl groups) has the largest effect in the stabilization of the adsorption process of Cd (Pb), respectively. These graphene oxide models shift the E_{ads} to be more stable by about 0.16 eV and 2.1 eV compared to pristine graphene for Cd and Pb, respectively. This finding asserts the role that these oxygen groups have on improving the adsorption process. Besides, our results suggest that the nature of Cd adsorption on graphene oxide is also mainly due to dispersive forces, however for Pb, there are some covalent bonding along with dispersion interactions. Finally, present studies provide a theoretical understanding of the interactions between some harmful heavy metals and graphene or graphene oxide which can be employed in water treatment applications of graphene-based nanomaterials.

CRediT authorship contribution statement

Sara M. Elgengehi: Visualization, Investigation, Writing - original draft. **Sabry El-Taher:** Supervision, Validation. **Mahmoud A.A. Ibrahim:** Software, Resources. **Jacques K. Desmarais:** Formal analysis, Resources. **Khaled E. El-Kelany:** Conceptualization, Data curation, Writing - review & editing, Supervision, Project administration.

Declaration of Competing Interest

The authors declare that they have no known competing financial interests or personal relationships that could have appeared to influence the work reported in this paper.

Acknowledgements

The authors acknowledge Science and Technology Development Fund (STDF), Egypt for their financial support to establish an HPC-unit at CompChem Lab, Minia University. As well, we acknowledge Compute Ontario (Graham) in partner with Compute Canada (www.computecanada.ca) for providing the necessary computational facilities.

References

[1] K.S. Novoselov, A.K. Geim, S.V. Morozov, D. Jiang, Y. Zhang, S.V. Dubonos, I.V. Grigorieva, A.A. Firsov, Electric field effect in atomically thin carbon films, Science 306 (2004) 666–669.

[2] P. Avouris, Graphene: Electronic and photonic properties and devices, Nano Lett. 10 (2010) 4285–4294.

[3] K.I. Bolotin, K.J. Sikes, Z. Jiang, M. Klima, G. Fudenberg, J. Hone, P. Kim, H.L. Stormer, Ultrahigh electron mobility in suspended graphene, Solid State Commu. 146 (2008) 351–355.

[4] X. Du, I. Skachko, A. Barker, E.Y. Andrei, Approaching ballistic transport in suspended graphene, Nat. Nanotechnol. 3 (2008) 491.

[5] A.K. Geim, Graphene: Status and prospects, Science 324 (2009) 1530–1534.

[6] X. Huang, X. Qi, F. Boey, H. Zhang, Graphene-based composites, Chem. Soc. Rev. 41 (2012) 666–686.

[7] X. Yu, H. Cheng, M. Zhang, Y. Zhao, L. Qu, G. Shi, Graphene-based smart materials, Nat. Rev. Mater. 2 (2017) 17046.

[8] C. Tabtimsai, T. Somtua, T. Motongsri, B. Wanno, A dft study of h_2co and hcn adsorptions on 3d, 4d, and 5d transition metal-doped graphene nanosheets, Struct. Chem. 29 (2018) 147–157.

[9] F. Schedin, A.K. Geim, S.V. Morozov, E.W. Hill, P. Blake, M.I. Katsnelson, K.S. Novoselov, Detection of individual gas molecules adsorbed on graphene, Nat. Mater. 6 (2007) 652.

[10] D.L. Carballeira, N. Ramos-Berdullas, I. Perez-Juste, J.L.C. Fajin, M.N.D.S. Cordeiro, M. Mandado, A computational study of the interaction of graphene structures with biomolecular units, Phys. Chem. Chem. Phys. 18 (2016) 15312–15321.

[11] X. Li, J. Yu, S. Wageh, A.A. Al-Ghamdi, J. Xie, Graphene in photocatalysis: A review, Small 12 (2016) 6640–6696.

[12] M. Hu, Z. Yao, X. Wang, Graphene-based nanomaterials for catalysis, Ind. Eng. Chem. Res. 56 (2017) 3477–3502.

[13] M.N. Groves, A.S.W. Chan, C. Malardier-Jugroot, M. Jugroot, Improving platinum catalyst binding energy to graphene through nitrogen doping, Chem. Phys. Lett. 481 (2009) 214–219.

[14] S.J. Zhang, S.S. Lin, X.Q. Li, X.Y. Liu, H.A. Wu, W.L. Xu, P. Wang, Z.Q. Wu, H.K. Zhong, Z.J. Xu, Opening the band gap of graphene through silicon doping for the improved performance of graphene/gaas heterojunction solar cells, Nanoscale 8 (2016) 226–232.

[15] Z.M. Ao, A.D. Hernández-Nieves, F.M. Peeters, S. Li, The electric field as a novel switch for uptake/release of hydrogen for storage in nitrogen doped graphene, Phys. Chem. Chem. Phys. 14 (2012) 1463–1467.

[16] M. Dragoman, D. Dragoman, Graphene-based quantum electronics, Prog. Quant. Electron. 33 (2009) 165–214.

[17] M.D. Stoller, S. Park, Y. Zhu, J. An, R.S. Ruoff, Graphene-based ultracapacitors, Nano Lett. 8 (2008) 3498–3502.

[18] R. Sordan, F. Traversi, V. Russo, Logic gates with a single graphene transistor, Appl. Phys. Lett. 94 (2009) 073305.

[19] Y. Qiu, Z. Wang, A.C.E. Owens, I. Kulaots, Y. Chen, A.B. Kane, R.H. Hurt, Antioxidant chemistry of graphene-based materials and its role in oxidation protection technology, Nanoscale 6 (2014) 11744–11755.

[20] F.M. Tonelli, V.A. Goulart, K.N. Gomes, M.S. Ladeira, A.K. Santos, E. Lorençon, L.O. Ladeira, R.R. Resende, Graphene-based nanomaterials: Biological and medical applications and toxicity, Nanomedicine 10 (2015) 2423–2450.

[21] S. Kim, C.M. Park, M. Jang, A. Son, N. Her, M. Yu, S. Snyder, D.-H. Kim, Y. Yoon, Aqueous removal of inorganic and organic contaminants by graphene-based nanoadsorbents: A review, Chemosphere 212 (2018) 1104–1124.

[22] S.C. Smith, D.F. Rodrigues, Carbon-based nanomaterials for removal of chemical and biological contaminants from water: A review of mechanisms and applications, Carbon 91 (2015) 122–143.

[23] K.C. Kemp, H. Seema, M. Saleh, N.H. Le, K. Mahesh, V. Chandra, K.S. Kim, Environmental applications using graphene composites: Water remediation and gas adsorption, Nanoscale 5 (2013) 3149–3171.

[24] S. Dubey, K. Gopal, J.L. Bersillon, Utility of adsorbents in the purification of drinking water: A review of characterization, efficiency and safety evaluation of various adsorbents, J. Environ. Biol. 30 (2009) 327–332.

[25] S. Wang, H. Sun, H.M. Ang, M.O. Tadé, Adsorptive remediation of environmental pollutants using novel graphene-based nanomaterials, Chem. Eng. J. 226 (2013) 336–347.

[26] K. Lü, G. Zhao, X. Wang, A brief review of graphene-based material synthesis and its application in environmental pollution management, Chinese Sci. Bull. 57 (2012) 1223–1234.

[27] W. Peng, H. Li, Y. Liu, S. Song, A review on heavy metal ions adsorption from water by graphene oxide and its composites, J. Mol. Liq. 230 (2017) 496–504.

[28] D. Gu, J.B. Fein, Adsorption of metals onto graphene oxide: Surface complexation modeling and linear free energy relationships, Colloid. Surf. A. Physicochem. Eng. Asp. 481 (2015) 319–327.

[29] S. Verma, R.K. Dutta, A facile method of synthesizing ammonia modified graphene oxide for efficient removal of uranyl ions from aqueous medium, RSC Adv. 5 (2015) 77192–77203.

[30] B. Feng, K. Xu, A. Huang, Covalent synthesis of three-dimensional graphene oxide framework (gof) membrane for seawater desalination, Desalination 394 (2016) 123–130.

[31] K. Nakada, A. Ishii, Dft calculation for adatom adsorption on graphene, in: J.R. Gong (Ed.), Graphene simulation, Technology Inc., Croatia, 2011, pp. 3–20.

[32] M. Manadé, F. Viñes, F. Illas, Transition metal adatoms on graphene: A systematic density functional study, Carbon 95 (2015) 525–534.

[33] X. Liu, C.Z. Wang, M. Hupalo, W.C. Lu, M.C. Tringides, Y.X. Yao, K.M. Ho, Metals on graphene: Correlation between adatom adsorption behavior and growth morphology, Phys. Chem. Chem. Phys. 14 (2012) 9157–9166.

[34] M. Hupalo, X. Liu, C.-Z. Wang, W.-C. Lu, Y.-X. Yao, K.-M. Ho, M.C. Tringides, Metal nanostructure formation on graphene: Weak versus strong bonding, Adv. Mater. 23 (2011) 2082–2087.

[35] I. Shtepliuk, N.M. Caffrey, T. Iakimov, V. Khranovskyy, I.A. Abrikosov, R. Yakimova, On the interaction of toxic heavy metals (cd, hg, pb) with graphene quantum dots and infinite graphene, Sci. Rep. 7 (2017) 3934.

[36] A. Hamed Mashhadzadeh, M. Ghorbanzadeh Ahangari, A. Salmankhani, M. Fataliyan, Density functional theory study of adsorption properties of non-carbon, carbon and functionalized graphene surfaces towards the zinc and lead atoms, Physica E. 104 (2018) 275–285.

[37] D.W. Boukhvalov, M.I. Katsnelson, Modeling of graphite oxide, J. Am. Chem. Soc. 130 (2008) 10697–10701.

[38] I. Shtepliuk, V. Khranovskyy, R. Yakimova, Insights into the origin of the excited transitions in graphene quantum dots interacting with heavy metals in different media, Phys. Chem. Chem. Phys. 19 (2017) 30445–30463.

[39] R. Dovesi, A. Erba, R. Orlando, C.M. Zicovich-Wilson, B. Civalleri, L. Maschio, M. Rérat, S. Casassa, J. Baima, S. Salustro, B. Kirtman, Quantum-mechanical condensed matter simulations with crystal, Wiley Interdiscip. Rev. Comput. Mol. 8 (2018) e1360.

[40] R. Dovesi, V.R. Saunders, C. Roetti, R. Orlando, C.M. Zicovich-Wilson, F. Pascale, B. Civalleri, K. Doll, N.M. Harrison, P.D. Bush, I.J. Arco, M. Llunell, M. Causà, Y. Noël, L. Maschio, A. Erba, R. M.S. Casassa,, Crystal17 user's manual, University of Torino, Torino, 2017.

[41] C. Adamo, V. Barone, Toward reliable density functional methods without adjustable parameters: The pbe0 model, J. Chem. Phys. 110 (1999) 6158–6170.

[42] J. Paier, M. Marsman, G. Kresse, Why does the b3lyp hybrid functional fail for metals? J. Chem. Phys. 127 (2007) 024103.

[43] J. Heyd, J.E. Peralta, G.E. Scuseria, R.L. Martin, Energy band gaps and lattice parameters evaluated with the heyd-scuseria-ernzerhof screened hybrid functional, J. Chem. Phys. 123 (2005) 174101.

[44] B. Metz, H. Stoll, M. Dolg, Small-core multiconfiguration-dirac–hartree–fock-adjusted pseudopotentials for post-d main group elements: Application to pbh and pbo, J. Chem. Phys. 113 (2000) 2563–2569.

[45] C. Gatti, V.R. Saunders, C. Roetti, Crystal field effects on the topological properties of the electron density in molecular crystals: The case of urea, J. Chem. Phys. 101 (1994) 10686–10696.

[46] R.S. Mulliken, Electronic population analysis on lcao–mo molecular wave functions. I, J. Chem. Phys. 23 (1955) 1833–1840.

[47] E.R. Davidson, S. Chakravorty, A test of the hirshfeld definition of atomic charges and moments, Theor. Chim. Acta 83 (1992) 319–330.

[48] G. Beata, G. Perego, B. Civalleri, Crysplot: A new tool to visualize physical and chemical properties of molecules, polymers, surfaces, and crystalline solids, J. Comput. Chem. 40 (2019) 2329–2338.

[49] S. Grimme, J. Antony, S. Ehrlich, H. Krieg, A consistent and accurate ab initio parametrization of density functional dispersion correction (dft-d) for the 94 elements h-pu, J. Chem. Phys. 132 (2010) 154104.

[50] S.F. Boys, F. Bernardi, The calculation of small molecular interactions by the differences of separate total energies. Some procedures with reduced errors, Mol. Phys. 19 (1970) 553–566.

[51] J. Scaranto, G. Mallia, N.M. Harrison, An efficient method for computing the binding energy of an adsorbed molecule within a periodic approach. The application to vinyl fluoride at rutile tio2(110) surface, Comput. Mater. Sci. 50 (2011) 2080–2086.

[52] K. Nakada, A. Ishii, Migration of adatom adsorption on graphene using dft calculation, Solid State Commun. 151 (2011) 13–16.

[53] H. Gao, J. Zhou, M. Lu, W. Fa, Y. Chen, First-principles study of the iva group atoms adsorption on graphene, J. Appl. Phys. 107 (2010) 114311.

[54] V. Zólyomi, Á. Rusznyák, J. Kürti, C.J. Lambert, First principles study of the binding of 4d and 5d transition metals to graphene, J. Phys. Chem. C 114 (2010) 18548–18552.

[55] K.T. Chan, J.B. Neaton, M.L. Cohen, First-principles study of metal adatom adsorption on graphene, Phys. Rev. B 77 (2008).

[56] N. Dimakis, F.A. Flor, A. Salgado, K. Adjibi, S. Vargas, J. Saenz, Density functional theory calculations on transition metal atoms adsorbed on graphene monolayers, Appl. Surf. Sci 421 (2017) 252–259.

[57] N. Dimakis, D. Valdez, F.A. Flor, A. Salgado, K. Adjibi, S. Vargas, J. Saenz, Density functional theory calculations on alkali and the alkaline ca atoms adsorbed on graphene monolayers, Appl. Surf. Sci 413 (2017) 197–208.

[58] J.M. García-Lastra, Strong dependence of band-gap opening at the dirac point of graphene upon hydrogen adsorption periodicity, Phys. Rev. B 82 (2010) 235418.

[59] F. Calle-Vallejo, J.M. García-Lastra, Tailoring the electronic structure of graphene for catalytic and nanoelectronic applications, 2011 International Symposium on Advanced Packaging Materials (APM), IEEE, 2011, pp. 1–6.

[60] P. Lambin, H. Amara, F. Ducastelle, L. Henrard, Long-range interactions between substitutional nitrogen dopants in graphene: Electronic properties calculations, Phys. Rev. B 86 (2012) 045448.

[61] K.E. El-Kelany, P. Carbonnière, A. Erba, M. Rérat, Inducing a finite in-plane piezoelectricity in graphene with low concentration of inversion symmetry-breaking defects, J. Phys. Chem. C 119 (2015) 8966–8973.

[62] H. He, J. Klinowski, M. Forster, A. Lerf, A new structural model for graphite oxide, Chem. Phys. Lett. 287 (1998) 53–56.

[63] A. Lerf, H. He, M. Forster, J. Klinowski, Structure of graphite oxide revisited, J. Phys. Chem. B 102 (1998) 4477–4482.

[64] L.B. Casabianca, M.A. Shaibat, W.W. Cai, S. Park, R. Piner, R.S. Ruoff, Y. Ishii, Nmr-based structural modeling of graphite oxide using multidimensional 13c solid-state nmr and ab initio chemical shift calculations, J. Am. Chem. Soc. 132 (2010) 5672–5676.

[65] A. Tararan, A. Zobelli, A.M. Benito, W.K. Maser, O. Stéphan, Revisiting graphene oxide chemistry via spatially-resolved electron energy loss spectroscopy, Chem. Mater. 28 (2016) 3741–3748.

[66] C. Hontoria-Lucas, A.J. López-Peinado, J.D.D. López-González, M.L. Rojas-Cervantes, R.M. Martín-Aranda, Study of oxygen-containing groups in a series of graphite oxides: Physical and chemical characterization, Carbon 33 (1995) 1585–1592.

[67] X. Gao, D.-E. Jiang, Y. Zhao, S. Nagase, S. Zhang, Z. Chen, Theoretical insights into the structures of graphene oxide and its chemical conversions between graphene, J. Comput. Theor. Nanos. 8 (2011) 2406–2422.

[68] T.-F. Yeh, J.-M. Syu, C. Cheng, T.-H. Chang, H. Teng, Graphite oxide as a photocatalyst for hydrogen production from water, Adv. Funct. Mater. 20 (2010) 2255–2262.

[69] M. Lundie, Ž. Šljivančanin, S. Tomić, Analysis of energy gap opening in graphene oxide, J. Phys. Conf. Ser. 526 (2014) 012003.